ACS OMEGA

Open Access

http://pubs.acs.org/journal/acsodf

Article

Experimental and Theoretical Survey of Intramolecular Spodium Bonds/σ/π-Holes and Noncovalent Interactions in Trinuclear Zn(II)-Salen Type Complex with OCN^- Ions: A Holistic View in Crystal Engineering

Dhrubajyoti Majumdar,* Antonio Frontera, Sourav Roy, and Dipankar Sutradhar

Cite This: *ACS Omega* 2024, 9, 1786−1797

Read Online

ACCESS | Metrics & More | Article Recommendations | Supporting Information

ABSTRACT: In this work, one new centrosymmetric trinuclear Zn(II) complex **1**, [{(OCN)Zn(L)}$_2$Zn], using a salen-type ligand (H_2L) in the presence of OCN^- was synthesized and characterized via elemental, spectral, SEM−EDX, and single-crystal X-ray diffraction (SCXRD) study. In **1**, SCXRD reveals two different stereochemical environments of zinc metal ions; one terminal Zn(II) center adopts square pyramidal geometries with the Addison parameter (τ) 0.095, and the central Zn(II) is tetracoordinated tetrahedral geometry. This article provides evidence of the significance and presence of spodium bonds (SpBs) in solid-state crystal structures involving a pseudotetrahedral environment of the central Zn-atom. X-ray structures reveal intramolecular Zn···O SpBs caused by the methoxy ($-OCH_3$) substituent O-atom adjacent to the coordinated phenoxy O-atom. These noncovalent interactions have been thoroughly studied using density functional theory calculations at the RI-BP86[2]-D3[3]/def2-TZVP level of theory that characterizes the nature of SpBs, including the Baders quantum theory of atoms-in-molecules "QTAIM", molecular electrostatic potential (MEP) surface, and noncovalent index plot (NCI). In addition, a unique complex-isomer-based theoretical model has been vividly employed to estimate the SpBs energy in the complex. Natural bond orbital (NBO) analysis also tries to establish the differentiation between σ-hole and π-hole SpBs' natures more authentically. The complex energy frameworks were used to investigate noncovalent interactions. To better understand the different intermolecular interactions, we conducted a Hirshfeld surface, which revealed N···H (15.4%) and O···H (9.1%) contacts and Zn···O (5.1%) (SpBs).

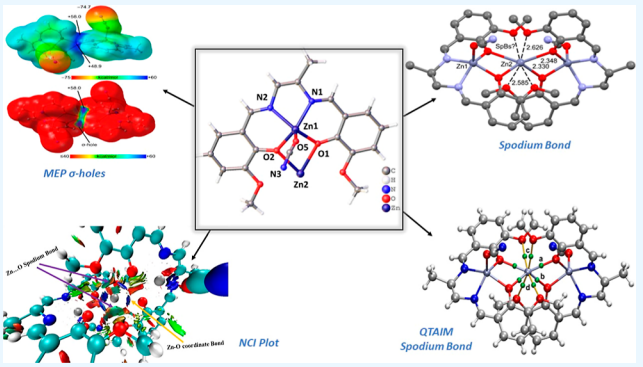

INTRODUCTION

There has been a rise in noncovalent interaction conceptions in crystal engineering over the past few decades, identified in the periodic table (Chart S1),[1] like hydrogen bonds (H-bond, X−H···Y).[2] Noncovalent interactions, specifically weak interactions (X−Z···Y), have been found to involve many of the main group elements (Z) (Scheme S1) following the initial discovery by renowned scientist J. D. van der Waals.[3] These interactions are now understood to be vital in living organisms, as evidenced by the double helix structure of DNA, attributed to van der Waals' discovery[3] and the structure of DNA itself.[4,5] The branch of supramolecular chemistry vividly explores various noncovalent interactions, including hydrogen bonding, C−H···π, π···π, van der Waals forces, ion−ion, dipole−dipole, and ion−dipole interactions.[6−9] Hydrogen bonding and π···π interaction are popular and extensively utilized in molecular chemistry and crystal engineering.[10−19] In solid-state environments, these interactions combine to create supramolecular structures through secondary bonds. While these bonds may not be durable in a solution, they are vital in constructing and designing crystal structures.[20] Even though noncovalent interactions are weaker than covalent interactions, they are essential in crystal engineering.[20,21] Researchers have recently discovered new types of noncovalent interactions worth exploring. There are two types of interactions known as σ- and π-hole.[22,23] The σ-hole interaction involves a negative site of an anion or a lone pair of a Lewis acid and a positive site for the extension of a covalently bonded atom.[24] In contrast, π-holes are positive electrostatic zones that form perpendicular to the σ-frame of a molecule. Molecular electrostatic potential (MEP) surface calculation is a practical approach to exploring

Received: October 25, 2023
Revised: November 13, 2023
Accepted: November 28, 2023
Published: December 19, 2023

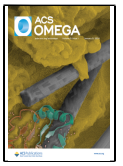

these interactions.[24] Now, these interactions are currently receiving much attention in supramolecular chemistry.[25] There have been postulations and legalizations of attractive interactions called "spodium bonds" (SpBs) between electron-rich atoms and any element of group 12 (Scheme S2).[1,20] In group 12 metal ions such as Zn, the coordination chemistry is fascinating with respect to crystal field stabilization energy (CFSE), which is primitive for other d^n electronic systems (n = number of d orbital electrons). Herein, the variation of coordination number and stereochemical arrangement is limited due to the d^{10} electronic system, which prevents the d−d transition. Besides, Zn(II) complexes exhibit prominent photoluminescence and electroluminescence properties and play a crucial role in many hydrolytic enzymes.[26] Scientists have recently begun researching SpBs using Zn(II) complexes, which has opened up a new avenue of research in contact with salen-type compartmental ligands.[20,24,27] The salen-type ligand (H_2L) is a potential N_2O_4 donor compartmental Schiff base with inner N_2O_2 and outer O_4 cavities. The ligand is intriguing in its ability to synthesize metal complexes since it encompasses two imines, two alkoxy's, and two phenolic −OH groups, which, after deprotonation, produce an N_2O_2 imine and phenoxide-type chelating position (Scheme S3) readily encapsulated metal ions in two different compartments.[26] Scheme S2 explores the SpB interaction between tetrahedral (left) and square-pyramidal (right) Zn(II) atoms, which provides a physical understanding of SpB that involves five coordinated Zn(II).[20] SpB interactions are not as strong as coordination bonds[21,25,28] and are sometimes called "pseudo-coordination" or "semicoordination."[20] Importantly, SpB interactions involve longer distances and the participation of an antibonding σ*orbital during complex formation, distinguishing them from coordination bonds.[1] This type of bonding involves commonly used noncovalent interactions, such as coinage, triel, tetrel, pnictogen, chalcogen, halogen, and noble gas bonding.[1,17] To explain such an unusual bonding feature, transition-metal ions (Zn), salen-type ligands, and OCN^- ions are used to frame coordination complexes that result in infinite arrays of various dimensions,[29−36] in which OCN^- ions bridging motifs result in multidimensional complex networks (Scheme S4).[37,38] Therefore, Zn(II)-salen type complexes with OCN^- ions are attractive due to the possibility of spodium bonding existence, which has not been well-researched.

This article reports synthesizing an X-ray-characterized centrosymmetric trinuclear Zn(II) complex with OCN^- ions using a salen-type ligand. The nature of spodium bonding has been investigated using density functional theory (DFT) calculations. The study was characterized using a combination of QTAIM, MEP surface, and noncovalent index (NCI) plots. The natural bond orbital (NBO) analysis aims to differentiate between the σ-hole and π-hole SpB in a new dimension. The interaction energy and Hirshfeld surface quantified the intermolecular interactions.

EXPERIMENTAL SECTION

Materials. The research chemicals and solvents (CH_3OH, DCM, and DMSO) used in this study were of reagent grade and were used without further purification. $Zn(OAc)_2.2H_2O$ (98%), KOCN (potassium cyanate) (96%), *ortho* vanillin ($C_8H_8O_3$) (99%), 1,2-propane diamine (99%), DCM (dichloromethane) (99.8%), and DMSO (99.9%) were purchased from the Sigma-Aldrich Company, USA.

Physical Measurements. The elemental compositions of the complex and ligands were analyzed using a PerkinElmer 2400 CHN elemental analyzer. KBr pellets were used and recorded using the PerkinElmer spectrum RX 1 and BRUKER RFS 27 models to obtain IR spectra. Raman spectral stretching was recorded by using the BRUKER RFS 27 model. The $^1H/^{13}C$ NMR spectral analyses were conducted on a Bruker 400 and 75.45 MHz FT-NMR spectrometer using TMS as a standard internal in DMSO-d_6 solvent. EDX was performed by using a W filament on the EDX OXFORD XMX N model. High-resolution SEM images were analyzed with the JEOL model JSM-6390LV. The Hitachi U-3501 model spectrophotometer was used to determine UV−visible spectra within the 200−800 nm range.

Synthesis of Ligand (H_2L). The salen-type ligand was obtained following the general method described in the references.[36] The standard synthetic protocol for the ligand is outlined below: 0.5 mmol 1,2-propane diamine (0.0371 g) was thoroughly mixed with 1 mmol *ortho* vanillin (0.152 g) in a methanol solvent. The resulting solution was refluxed for ca. 2 h and allowed to cool. The yellow-colored product separated upon cooling the overall solution and was collected. Finally, the product was air-dried. Yield: (90%), Anal. Calcd for $C_{19}H_{22}N_2O_4$: C, 66.65; H, 6.48; N, 8.18. Found: C, 65.88; H, 6.51; N, 8.14%. IR (KBr cm^{-1}) selected bands: ν(C═N), 1631, ν(C−N) 1205, ν(C−$O_{phenolic}$) 1251, ν(C−H) 727, ^1H NMR (DMSO-d_6, 400 MHz): δ (ppm) 13.65 (m, 1H, OH), 8.54−8.52 (s, 1H, N═CH), 6.76−7.02 (m, 8H, Ar-H), 3.59−3.75 (t, 2H, N−CH_2),and 2.51 (m, 2H, CH_2), ^{13}C NMR (DMSO-d_6, 75.45 MHz): δ (ppm) 114.99−123.62 (Arom-C), 148.36−166.67 (C−OH), 167.55 (CH═N), UV−vis λ_{max} (CH_3OH) 283 and 334 nm.

Synthesis of Complex [{(OCN)Zn(L)}$_2$Zn] 1. $Zn(OAc)_2.2H_2O$ (0.219 g, 1 mmol) was dissolved in 30 mL of hot methanolic solution of ligand (H_2L) and refluxed for about 1 h. After that, an aqueous methanolic (5 mL) solution of KOCN (0.081 g, 1 mmol) was added dropwise. Then the resultant solution mixture was stirred at room temperature for 1.5 h, followed by 4 mL of DCM + DMSO (1:1 v/v) added dropwise to this reflux solution and further stirred at 80 °C for 2 h under ice-bath conditions. The light-yellow solution was filtered and kept at room temperature for slow crystallization. After a few days, needle-sized, light, yellow-colored single crystals suitable for single-crystal X-ray diffraction (SCXRD) were obtained. After rinsing thoroughly with cold ether to eliminate contaminants, the crystals were isolated by filtration and then air-dried in a desiccator. Yield: 0.410 g, (53%), Anal. Calcd for $C_{40}H_{36}Zn_3N_6O_{10}$: C, 50.21; H, 3.79; N, 8.78. Found: C, 50.17; H, 3.74; N, 8.80%. FT-IR (KBr cm^{-1}) selected bands: ν(OCN) in KOCN, 2176 s, for complex, ν(C═N), 1620 s, ν(OCN), 2182 m, ν(C−$O_{phenolic}$) 1249 s, ν(C−N) 1200, ν(C−H) 715, FT-Raman (cm^{-1}) selected bands: ν(OCN) in KOCN, 2175 s, for complex, ν(C═N), 1648 s, ν(OCN), 2180, ν(C−$O_{phenolic}$)1210, ν(C−H) 718,^1H NMR (DMSO-d_6, 400 MHz)Z δ (ppm) 2.07 (s, 3H), 6.30−7.35 (w, Arom-H), 8.31 (w, 1H), and 3.67 (m, 2H), UV−vis λ_{max} (DMF) 278 and 321 nm.

X-ray Crystallography. The complex in crystal form was grown in situ by self-assembly after the slow evaporation of the CH_3OH + DCM + DMSO mixed solvent at room temperature. The SCXRD data were collected on a Bruker CCD[39] diffractometer using Mo Kα radiation at λ = 0.71073 Å. We utilized various crystallographic programs to determine the

https://doi.org/10.1021/acsomega.3c08422
ACS Omega 2024, 9, 1786−1797

Scheme 1. Synthetic Route for Ligand and Complex

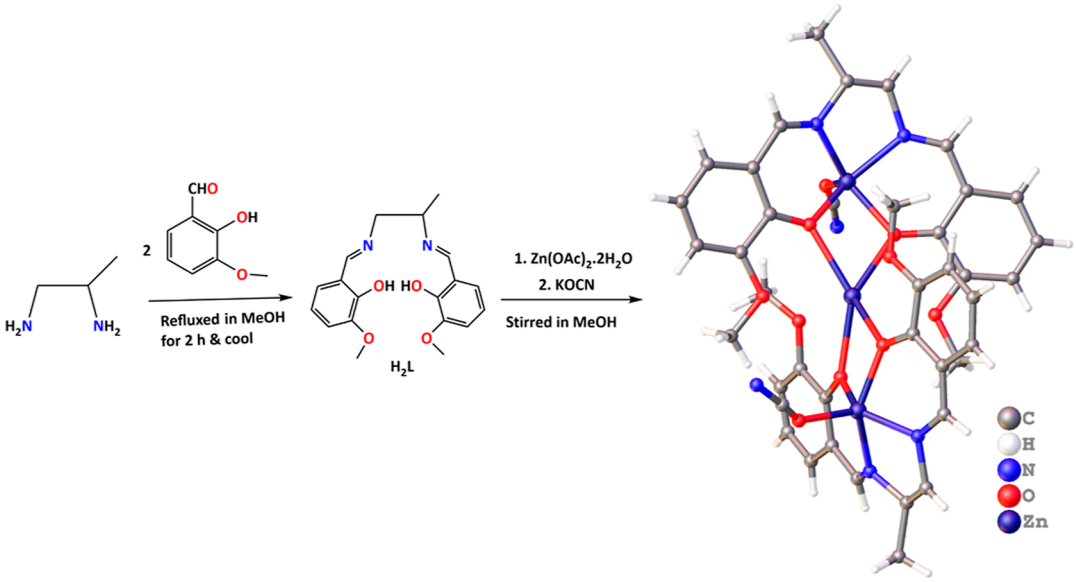

complex crystal structure. To gather relevant data, SMART detects information frames, analyzes reflections, and determines lattice parameters. SAINT[40] combines the intensity of reflections and scales them, while SADABS[41] corrects for absorption. Finally, the space group, structure, and F^2 were determined using SHELXTL through least-squares methods. The crystal structure was solved using full-matrix least-squares methods against F^2, with the help of SHELXL-2014[42] and Olex-2 software.[43] To refine all non-hydrogen atoms, we utilized the anisotropic shift parameters. A sensitive isotropic was achieved after fixing the hydrogen positions at their calculated positions. The crystal structure possesses a B-level alert. The alert level alert in the check-cif was resolved in the following manner: the alert was due to bad quality data. We crystallized several times to obtain better-quality data for this structure; however, due to poor crystal quality, the wR^2 value is high. We are confident that the crystal structural characterization and data from the best crystal are valid. The CCDC reference number 2265592 is for the complex. The various crystallographic molecular diagrams have been constructed employing the latest version of Diamond's software. The essential crystallographic information and complete structure refinement parameters are shown in Table S1, whereas some important bond angles (deg) and distances (Å) are summarized in Table S2.

Theoretical DFT Methods. The single-point calculation and optimizations were carried out using the Turbomole 7.7 program[44] and the RI-BP86[2]-D3[3]/def2-TZVP[45] level of theory. Bader's "Atoms in molecules" theory (QTAIM)[46] was used to study the interactions discussed herein using the Multiwfn program[47] and represented using the VMD visualization software.[48] For the representation of the MEP surface, the 0.001 au iso-surface was used to emulate the van der Waals surface. Further, DFT-based wB97XD[49] functional in conjugation with def2-TZVP have been used to compute the interaction energies of the complex. It should be noted that the coordinates obtained from the SCXRD structure have been used to perform all of the electronic structure calculations. NBO analysis[50] was done to get ideas about electronic rearrangements, charges on individual atoms, and second-order hyperconjugation energy. All electronic structure calculations were carried out using the Gaussian09 suite of programs.[51]

Hirshfeld Surface. Hirshfeld surfaces[52−54] and two-dimensional (2-D) fingerprint plots[55,56] have been calculated using Crystal Explorer software.[57] The bond lengths of the hydrogen atoms have been set to standard values. d_e and d_i are defined for each point on the Hirshfeld surface to calculate the normalized contact distance (d_{norm}) using the appropriate formula. The d_{norm} value depends on the relative values of intermolecular contacts and van der Waals separations. The HS with a red-white-blue color scheme is displayed with the d_{norm} parameter. The map's colors indicate varying contact levels: red for shorter contacts, white for contacts at the van der Waals separation, and blue for no contact at all.

RESULTS AND DISCUSSION

Synthetic Perspective and Ligand Overview. The ligand was synthesized using the published literature method (Scheme 1).[36] The complex was obtained using a methanolic solution of ligand and $Zn(OAc)_2{\cdot}2H_2O$ in the presence of a few drops of aqueous KOCN, yielding a moderately satisfactory yield through the self-assembly in situ synthetic method. To achieve high-quality crystals suitable for SCXRD, we added a small amount of DCM + DMSO mixture (1:1, v/v) to the methanol solvent during the crystal growth. The process helped to improve the crystal diffraction quality. The prepared light-yellow crystal complex is insoluble in water and soluble in organic solvents like DMF, DMSO, and so forth. They are moderately stable and sensitive to air and moisture. The literature on SpB analysis in association with the σ- and π-hole of zinc metal complexes involving compartmental salen-type ligands is limited, with only a few researchers exploring SpB's nature using analogous reduced Schiff bases or similar compartmental ligand complexes.[24,27,58] Therefore, research on spodium bonding, particularly with compartmental salen-type ligands, is attractive to synthetic chemists.

Spectroscopic Characterization. *FT-IR and Raman Spectroscopy.* It has always been crucial for synthetic chemists to characterize newly synthesized compound structures based on spectroscopy. Therefore, we prioritized the synthesized

https://doi.org/10.1021/acsomega.3c08422
ACS Omega 2024, 9, 1786−1797

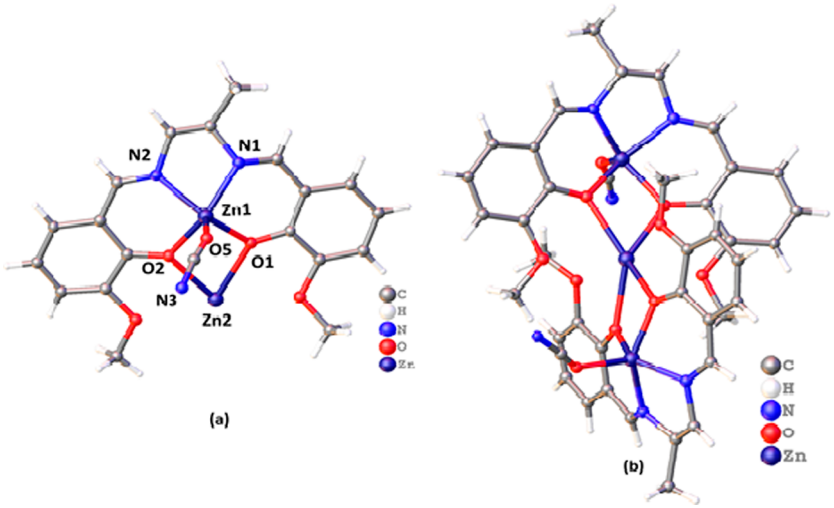

Figure 1. Perspective view of complex **1**. (a) Asymmetric unit with selective atom numbering scheme and (b) complex **1** (ball and stick style).

complex by IR analysis and Raman spectra. In this discussion, we will compare the IR spectral characteristics of OCN^- (KOCN salt used during complex synthesis) with those of coordinated OCN^- ions with zinc metals in the complex (Scheme S3).[37,59,60] The azomethine linkage in the complex was identified at 1620 cm^{-1} compared to the salen ligand at 1631 cm^{-1} (Figure S1,S1A).[32−37] Notably, the IR spectra of the OCN^- ions in standard KOCN salts show strong bands near 2176 cm^{-1} (Figure S1B),[59−61] while in the zinc metal complex with O-coordinated stretching of OCN^- ions were observed at 2182 cm^{-1} (Figure S1A).[59−61] The comparative IR spectral approach helps to determine whether or not OCN^- can link with zinc metal ions and that this linking occurs through an O-atom. The bonding properties of OCN^- are like those of the literature-published complexes.[37,59−61] We also characterized the complex using Raman spectra. The Raman peak identified the azomethine linkage in the complex at 1648 cm^{-1}. In the OCN^- in KOCN salt, Raman peak at 2175 cm^{-1} (Figure S2A), whereas in the complex, the Raman peak at 2180 cm^{-1} (Figure S2).[62] The appearance of the Raman peak at 2180 cm^{-1} ensures OCN^- joined with zinc metals in the complex via O-atom.

UV Spectrum. We conducted a UV−visible spectral study to examine the salen-type ligand and its complex. The ligand's spectrum was taken in methanol, while the complex was tested in DMF solvent (Figure S3). Based on the spectral results, we found that the ligand had peaks at 283 and 334 nm,[32−37] while the complex had significant peaks at 278 and 321 nm.[27] According to the findings, two electronic transitions arise from the ligand and the complex. The coordination of zinc metal ions with the ligand changes the spectrum. It is worth noting that different complexes of Zn(II)-salen type ligands exhibit analogous UV−visible spectral characteristics.[27,34,35]

^1H and ^{13}C NMR Spectra. A successful NMR spectroscopic study, typically using $^1H/^{13}C$ NMR, was conducted to investigate the recently synthesized salen-type ligand and its complex in-depth structure. The ^1H NMR spectroscopic study identifies the type of proton nuclei, while ^{13}C NMR identifies the carbon atoms in the synthesized compounds. The experimental $^1H/^{13}C$ NMR chemical shifts of the salen-type ligand and the complex taken in DMSO-d_6 solvent are detailed under the Experimental Section referencing TMS. We can rely on the structural studies of the salen-type ligand and the complex provided in clubbed Figures S4 (for ligand)−S6 (for complex) to determine the essential peaks for NMR spectra. In the case of the salen-type ligand, ^1H NMR spectra initially identify free phenolic-OH and other significant proton nuclei. In contrast, the ^{13}C NMR spectral study primarily identifies the carbon framework in the ligand structure. The ligands possess free phenolic proton (OH) peaks identified by the chemical shift of 13.65 ppm. The azomethine linkage formation (CH═N) supports the successful Schiff base synthesis, and such azomethine proton chemical shifts were observed at 8.52−8.54 ppm, whereas the aromatic ring protons resonate at 6.76−7.62 ppm.[63,64] In addition, the experimental NMR peak at 2.51 ppm is assigned to the CH_3 group protons. In the case of the complex, we examined whether the ligand phenolic −OH group is coordinated with zinc metal ions. Herein, the OH proton signal on the ligand disappeared in the ^1H NMR spectra of the complex, indicating deprotonation and coordination of the O atom with the Zn metal ion.[63,64] Additionally, the analysis of ^{13}C NMR distinguishes and identifies carbon atoms in aromatic rings, azomethine, and other areas. The carbon resonances for azomethine (CH═N) in the ^{13}C NMR spectrum are 167.55 ppm, while the aromatic carbon shifts are 114.99−123.62 ppm.

SEM−EDX Analysis. Scanning electron microscopy (SEM) is a popular and common method that uses high-energy electrons focused on a sample's surface to identify nanomaterials. The technique produces specific signals visible through SEM on the surface of the solid pieces. When these signals are received and processed, they cause interactions between the electrons and the sample. This interaction reveals the sample's (here crystal complex) external texture, material orientation, crystal structure, and chemical composition.[65] The SEM micrographs for the prepared compound explored the ice crystal morphology, showing that the morphology is distributed in overlapping sheets (Figure S8). Similarly, the energy-dispersive X-ray spectroscopy (EDX) system adds to electron microscopy equipment, specifically SEM or TEM equipment. It helps to identify samples by using the imaging capability of the microscope. The EDX spectrum shows a range of peaks that correspond to elements present in the compound. This information reveals the types of atoms in the complex and their percentage composition within its structure (Table S3). The spectrum of the synthesized complex indicates

https://doi.org/10.1021/acsomega.3c08422
ACS Omega 2024, 9, 1786−1797

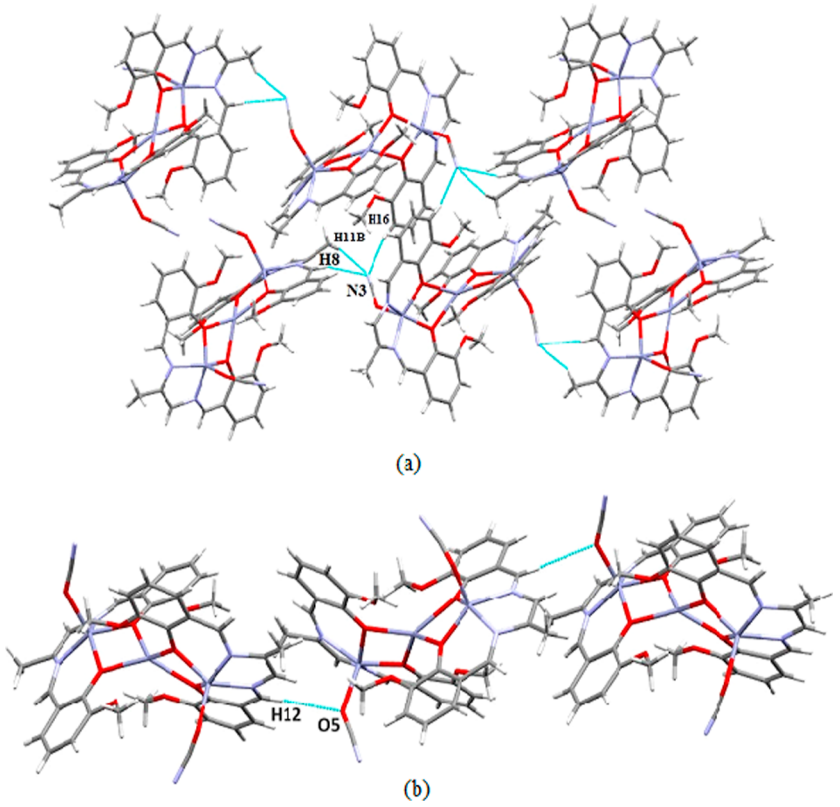

Figure 2. (a) Perspective view of weak hydrogen bonding interaction in complex **1**. (b) Perspective view of weak C−H···O interaction in complex **1** (all are selective atom numbering scheme).

the presence of C, O, and K/Zn metals, which suggests that the desired synthesis complex was booming (Figure S7). Here, K must come from KOCN, which is used during complex crystal preparation. The elements C and O are also derived from the organic Schiff base ligand framework.[66]

Crystal Structure Description. The X-ray crystal structure determination revealed that complex **1** crystallizes in the orthorhombic space group *Pbcn*. A perspective view of the complex [asymmetric unit (a)] is given in Figure 1. Details of the crystallographic data and refinement are given in Table S1. Some important bond lengths (Å) and bond angles (deg) are given in Table S2. The complex is centrosymmetric and built from an isolated trinuclear unit of $[\{(OCN)Zn(L)\}_2Zn]$, where two terminal "metalloligands"[65] (ZnL) are aligned at an angle of ∼75°, which are bridged to central zinc, Zn(2) forming the trinuclear core. The cyanate coligand coordinates to the zinc(II) of ZnL moiety, which now acts as a terminal "metalloligands" (ZnL), and two of these metalloligands coordinate with a second zinc(II), resulting in $[\{(OCN)Zn(L)\}_2Zn]$. Interestingly, the terminal zinc centers are pentacoordinated, whereas the central zinc center is tetracoordinated. The zinc(II) centers [Zn(1) and Zn(1)*] are coordinated with two imine nitrogen atoms [N(1), N(2) for Zn(1) and N(1)*, N(2)* for Zn(1)*] and two phenoxo oxygen atoms [O(1), O(2) for Zn(1) and O(1)*, O(2)* for Zn(1)*] of the deprotonated Schiff bases (salen type) [* = 1 − x, y, 1.5 − z]. An oxygen atom occupies the fifth site [O(5) for Zn(1) and O(5)* for Zn(1)*] from cyanate coligand. The terminal zinc(II) centers adopt square pyramidal geometries with the Addison parameter (τ) ∼0.095. The central zinc(II), Zn(2), is tetracoordinated and adopts tetrahedral geometry.[67] Due to the nearly perpendicular binding of the terminal metalloligands toward Zn(2), the methoxy oxygens are situated at a larger distance, hindering them from establishing covalent bonds with Zn(2); rather, noncovalent interactions (SpBs) are established, which hold the structure and provide stability. We ensure that the spodium bonding features are rare in the Zn(II)-salen-type complexes with OCN^- ions (Table S4). The trans angles, {N(1)−Zn(1)−O(2) and N(2)−Zn(1)−O(1)} in the complex, are found to be 145.2°(5) and 138.8°(4), respectively. The distance between the zinc(II) centers is close to 3.47 Å. Moreover, Zn(II)−O−Zn(II) angles are ∼105°. Three zinc(II) centers sit in a plane, forming an angle close to 180° (∼179.6°). In the complex, Zn(II)−OCN^- bond distances are comparable to the literature-published zinc metal complexes.[59,60]

Solid-State Supramolecular Interactions. We have found solid-state supramolecular interactions in the crystal structure of the complex. The crystal packing consists of weak C−H···N interactions. The OCN^- nitrogen forms three weak hydrogen bonding interactions with three hydrogen atoms, H(8), H(11B), and H(16), attached to carbon atoms, C(8), C(11), and C(16), respectively. These interactions result in the formation of a 2D structure, as shown in Figure 2a. The details of the geometric features are listed in Table 1.

Apart from C−H···N interactions, weak C−H···O interactions are observed. A hydrogen atom, H(12), attached to a carbon atom, C(12), forms a weak C−H···O interaction with a symmetry-related (1/2 − x, −1/2 + y, z) oxygen atom, O(5), from a cyanate ligand forming a 1-D structure (Figure 2b) [H···A = 2.795(3) Å, ∠D−H···A = 174°].

Hirshfeld Surface. The Mercury software contact analysis indicates that the complex has multiple contacts and supramolecular interactions, which were further studied

https://doi.org/10.1021/acsomega.3c08422
ACS Omega 2024, 9, 1786−1797

Table 1. Hydrogen Bond Distances (Å) and Angles (deg) of the Complex[a]

D−H···A	D−H	H···A	D···A	∠D-H···A
C(8)−H(8)−N(3)[b]	0.93	2.58	3.45(3)	155
C(11)−H(11B)−N(3)[b]	0.96	2.38	3.19(3)	142
C(16)−H(16)−N(3)[c]	0.93	2.49	3.29(3)	144

[a]D = donor; H = hydrogen; A = acceptor. [b]=1/2 − *x*, 1/2 − *y*, 1/2 + *z*. [c]=1 − *x*, 1 − *y*, 1 − *z*.

through Hirshfeld surface analysis (HSA). HSA provides an overall understanding of the electronic distribution over the complex. Two-dimensional fingerprint plots have been established from d_e and d_i, presenting the intermolecular contacts/interactions in the complex structure. The Hirshfeld surface of the complex has been mapped with the help of d_{norm} (−0.5 to 1.5 Å), shape index (−1.0 to 1.0 Å), curvedness (−4.0 to 0.4 Å), and fragment patch (0 to 15 Å), as shown in Figure 3. The deep blue and red circular zone on the d_{norm} Hirshfeld surfaces reveal shorter and longer inter-contacts and vice versa. In contrast, the white zone on the surfaces specifies the van der Waals radii contacts. The major bright red region on Hirshfeld surface plots is N···H (15.4%) and the O···H (9.1%) contacts. It is to be mentioned that the SpB interactions are also observed, Zn···O (5.1%), in Hirshfeld surface plots, as shown in Figure 3.

Calculations of Interaction Energy and Energy Frameworks. The energy calculation, HF/3-21G, available in Crystal Explorer 17 has been used to calculate the intermolecular interaction energies (Table 2), where a cluster of molecules is generated by applying crystallographic symmetry operations concerning a selected central molecule within the radius of 3.8 Å by default.[68] The total intermolecular energy (E_{tot}) is the sum of electrostatic (E_{ele}), polarization (E_{pol}), dispersion (E_{dis}), and exchange-repulsion (E_{rep}) energies with scale factors of 1.019, 0.651, 0.901, and 0.811, respectively.[69] The calculated interaction energies (kJ/mol) are −189.7 (E_{ele}), −198 (E_{pol}), −274.4 (E_{dis}), 151.8 (E_{rep}), and −446.5 (E_{tot}). Table 2 lists the calculated interaction energies in kJ/mol and the symmetry operations for 15 complex molecules. The molecule located at 4.56 Å from the centroid of the selected molecule shows the highest total interaction energy (−120.1 kJ/mol), whereas the molecule at 13.72 Å from the centroid of the selected molecule exhibits the lowest total interaction energy (−2.0 kJ/mol). The dispersion energy has a clear dominance over the other interaction energies (Figure 4); this is because of the presence of atoms with higher electrons/electron clouds (metal atoms). With an increasing number of electrons in an atom or molecule, the dispersion force will be stronger. This also suggests that the crystal packing mainly consists of nontraditional interactions (SpB). The electrostatic energy is lower due to the absence of strong hydrogen bonds. Only weak hydrogen bonds are observed in the complex. The energy frameworks represent the intermolecular interaction energies with their magnitude in a pictorial way.[70] Energies between molecular pairs are represented as cylinders joining the centroids of pairs of molecules. The cylinder radius is proportional to the relative strength of the corresponding interaction energy.[71] Energy frameworks are constructed for E_{ele} (red cylinders), E_{dis} (green cylinders), and E_{tot} (blue cylinders) (Figure 4).

SpBs Overview and Investigations. In this complex, the prime theoretical investigation is devoted to the study of

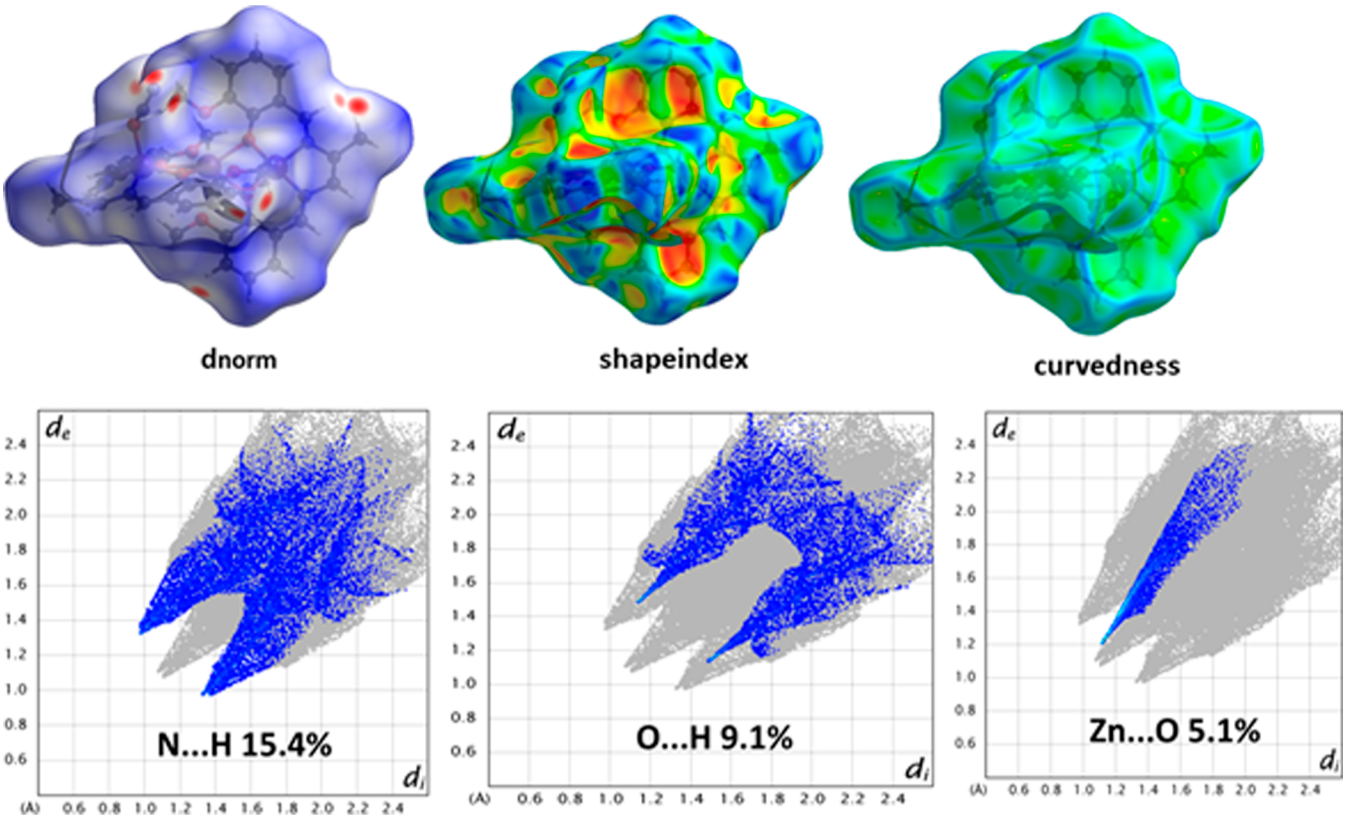

Figure 3. HS mapped with d_{norm}, shape index, curvedness (top), and a 2-D fingerprint plot for the corresponding interactions (bottom) of the complex.

https://doi.org/10.1021/acsomega.3c08422
ACS Omega 2024, 9, 1786−1797

Table 2. Different Interaction Energies of the Molecular Pairs (kJ/mol)

N	symmetry operations	R (Å)	electron density	E_{ele}	E_{pol}	E_{dis}	E_{rep}	E_{tot}
0	$-x + 1/2, y + 1/2, z$	8.25	HF/3-21G	−8.6	−10.2	−35.0	8.4	−40.2
0	$x, -y, z + 1/2$	11.97	HF/3-21G	−9.0	−16.1	−8.8	5.3	−23.3
0	$x + 1/2, y + 1/2, -z + 1/2$	12.24	HF/3-21G	4.9	−2.2	−9.9	1.6	−4.1
0	$x + 1/2, y + 1/2, -z + 1/2$	11.68	HF/3-21G	1.9	−2.6	−8.4	3.9	−4.1
0	$-x + 1/2, y + 1/2, z$	8.22	HF/3-21G	−8.6	−10.2	−35.0	8.4	−40.2
0	$x, -y, z + 1/2$	11.85	HF/3-21G	−9.0	−16.1	−8.8	5.3	−23.3
0	$-x + 1/2, -y + 1/2, z + 1/2$	9.70	HF/3-21G	−46.0	−36.1	−23.4	25.0	−71.2
0	$-x, -y, -z$	13.72	HF/3-21G	5.9	−2.0	−11.8	4.9	−2.0
0	$-x, y, -z + 1/2$	5.08	HF/3-21G	0.0	0.0	0.0	0.0	0.0
0	$x, -y, z + 1/2$	9.14	HF/3-21G	−4.0	−4.4	−19.3	6.2	−19.3
0	$-x, -y, -z$	9.32	HF/3-21G	−74.0	−52.8	−53.0	46.1	−120.1
0	$x + 1/2, y + 1/2, -z + 1/2$	12.27	HF/3-21G	1.9	−2.6	−8.4	3.9	−4.1
0	$-x + 1/2, -y + 1/2, z + 1/2$	9.85	HF/3-21G	−46.0	−36.1	−23.4	25.0	−71.2
0	$x + 1/2, y + 1/2, -z + 1/2$	11.71	HF/3-21G	4.9	−2.2	−9.9	1.6	−4.1
0	$x, -y, z + 1/2$	8.98	HF/3-21G	−4.0	−4.4	−19.3	6.2	−19.3

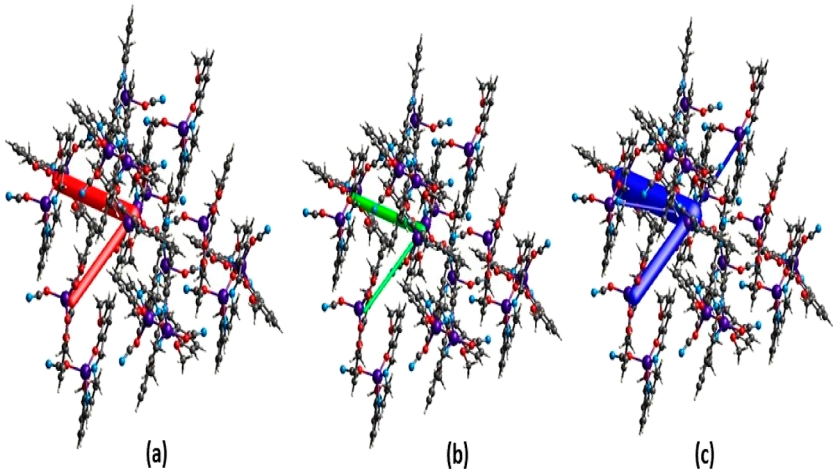

Figure 4. Perspective views of electrostatic energy (a), dispersion energy (b), and total energy diagrams (c) constructed from the energy framework for a cluster of molecules in the complex (the cylindrical radius is proportional to the relative strength of the corresponding energies, scale factor used is 100 with cutoff values of 10 kJ/mol).

intramolecular SpBs,[1] observed in the central (pseudo tetrahedral) Zn-atom of the trinuclear complex (Figure S9). This Zn2 is bonded to four bridging phenolate O atoms to form a distorted tetrahedron. Zn1 is situated in a distorted square pyramidal environment where the ligand [O1, N1, N2, O3] donor atoms form the pyramid's base, and O5 of the cyanate ligand is at the apex. The Zn2−O coordination distances are 2.348 and 2.330 Å (Figure S9). These distances can be considered normal Zn−O coordination bonds.[72] The Zn···O distances where the O-atom belongs to the methoxy substituent of the aromatic ring are 0.7−0.8 Å longer than ΣRcov (Zn + O) and, consequently, can be considered as intramolecular SpBs, as further analyzed below. These interactions are depicted in Figure S9 as black dashed lines. It is worth emphasizing that the Zn atom establishes a total of eight Zn···O bonds (coordination and SpBs), which is quite rare.

QTAIM Analysis. To characterize the SpBs in the complex, we performed QTAIM analysis, shown in Figure S10. For clarity, only the bond critical points (CPs, represented as green spheres) and bond paths (solid orange lines) interconnecting the Zn2 ion to the surrounding O-atoms have been plotted. It can be observed that the QTAIM confirms that the Zn-atom is connected to the eight O-atoms (four phenoxy and four methoxy O-atoms). The two pairs of bond CPs that characterize the SpBs have been labeled as "**c**" and "**d**," and the two pairs of bond CPs that depict the four Zn−O coordination bonds have been tagged as "**a**" and "**b**." The QTAIM parameters measured at bond CPs **a**−**d** are summarized in Table 3. The values of $\rho(r)$ and the Laplacian of $\rho(r)$ at the bond CPs that characterize the SpBs (**c**, **d**) are significantly smaller than those at the coordination bonds. The values at the bond CPs corresponding to SpBs are in the range of typical noncovalent interactions. The same behavior is observed for the smaller energy densities of the SpBs compared to coordination bonds. Another interesting result is that the total energy density, H(r), is minimal in the CPs labeled as "**b**"

Table 3. Electron Charge Density (ρ), Its Laplacian ($\nabla^2\rho$), Kinetic (V), Lagrangian (G), and Total (H) Energy Densities at the Bond CPs Labeled in Figure 6 in au

complex	ρ	$\nabla^2\rho$	V	G	H
a	0.03582	0.12656	−0.03598	0.03381	−0.0022
b	0.03727	0.13416	−0.03814	0.03584	−0.0023
c	0.02092	0.06514	−0.01767	0.01698	−0.0007
d	0.01914	0.05773	−0.01566	0.01504	−0.0006

https://doi.org/10.1021/acsomega.3c08422
ACS Omega 2024, 9, 1786−1797

and "c" (as it is typical in weak interactions) and negative in the coordination bonds, which is an indication of significant covalent character in the coordination bonds.[27,73]

Complex Isomer Used to Estimate SpB Energy: A Novel Theoretical Approach. Several theoretical models and isomers have been used to estimate the SpBs energy in the compound (Scheme S5). First, an isomer of the model of the complex (denoted as **1a**) has been constructed where the methoxy group is located para instead of ortho to the phenolate O-atom. In this complex, the SpBs cannot be formed, while the basicity of the phenolate atoms is like that of **1** (electron donor substituent in para instead of ortho). The energy difference between the isomeric forms could be attributed to the contribution of the SpBs but only in the case where both isomers were isoenergetic. To check this, the mononuclear models **1′** and **1a′** were also computed, revealing that the ligand with the methoxy in the para position is energetically favored −3.6 kcal/mol compared to the ligand with the methoxy group in the ortho position. Since the transformation of compound **1** to its isomeric form **1a** involves two ligands, the isomer **1a** should be −7.2 kcal/mol more stable than **1**, taken without considering any other effect. However, isomer **1a** is only −3.4 kcal/mol, and the difference to −7.2 kcal/mol can be ascribed to the impact of the formation of the SpBs, that is, −3.8 kcal/mol. Using this indirect procedure, it can be concluded that the strength of the SpBs is around −1 kcal/mol. The contribution of the SpBs in **1** is smaller than that obtained for similar systems. A likely explanation is that the fully optimized structure of compound **1** differs from the experimental one in two important aspects (Figures S9 and S11). One factor is that the coordination bonds shorten compared to the experimental one, with a concurrent enlargement of two SpB atoms (3.066 Å). The other two SpBs present a Zn···O distance (2.674 Å) that is very similar to that of the experimental one (2.626 Å). Therefore, the estimation of the SpBs using the fully optimized isomer is, in fact, evaluating only two SpBs instead of four. This result also highlights the unexpected behavior of the central Zn-atom that can establish four concurrent SpBs using the four σ-holes opposite to the four coordination Zn−O bonds, generating a pseudo coordination number of eight. We searched SpBs features in the literature on related complexes and found that SpBs bonding features in Zn(II)-salen-type complexes with OCN^- ions are rarely seen (Table S4). The claim regarding noncovalent interactions (SpBs) providing structural stability has been supported theoretically through DFT calculations. Experimental proof of this stability is challenging to obtain. The X-ray structure serves as the primary supporting evidence. As a compromise, we have modified the sentence to state, 'noncovalent interactions (SpBs) are established, most likely contributing to stability, as indicated by the DFT analysis.'

Noncovalent Interaction Index. The nature of SpBs can be further elaborated based on in-depth NCI plot analysis. The difference between the nature of the Zn−O coordinate bond and Zn···O noncovalent bond can be easily identified from the bond distance and the charges on each oxygen atom. The Zn1···O1 and Zn1···O2 interactions are found to have an intramolecular distance of 2.585 Å, whereas Zn1···O3 and Zn1···O4 are characterized with 2.626 Å. In comparison, the Zn1−O coordinate bonds are described with 2.330 and 2.348 Å. An intramolecular Zn···O distance of and around 2.6 Å is predicted for various Zn···O SpBs in two recently reported Zn-complex.[27] Our predicted complex Zn···O distances are very close to the previously reported values indicating the existence of similar Zn···O SpBs. Moreover, a clear distinction is also observed in the charges of oxygen atoms (−0.832 and −0.853 e), which are coordinated to Zn, then to those oxygens (−0.485 and −0.483 e) noncovalently bonded to Zn atom. Moreover, a NCI calculation shown in Figure 5 also confirms the distinctive feature of Zn···O interaction over the Zn−O bond. These results ensure a noncovalent interaction (SpBs) involving Zn1 with O1, O2, O3, and O4.

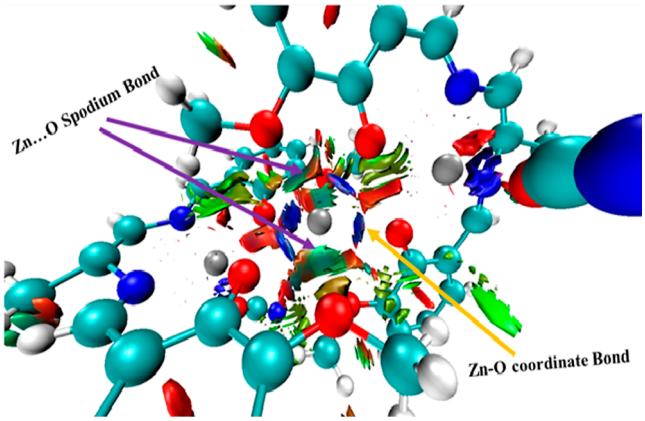

Figure 5. NCI picture showing Zn···O SpB and Zn−O coordinate bond (the Zn···O SpB is characterized with a lighter greenish patch, whereas Zn−O coordinate bonds are shown with prominent blue colors).

MEP Surface-Based σ-Holes Investigations. We used a theoretical model of the complex (Scheme S5) to explore whether there are σ-holes present in the central Zn atom. Using such a model is necessary because the σ-holes at Zn2 are "hidden" because of their interaction with the electron-rich O-atoms in the fundamental X-ray structure. In this model, the aromatic rings were eliminated to leave enolates as bridging ligands instead of phenoxides. The MEP surface of the model system using the default scale (top of Figure 6) shows that the MEP minimum is located at the N atom of the OCN^- ligand (−74.7 kcal/mol) and the maximum at the central Zn-atom, with a certain degree of anisotropy. Plotting the MEP on a different scale reveals four patches of electropositive potential (+58 kcal/mol), two of them visible in Figure 6 (bottom) and another two (symmetrically equivalent) at the opposite side (not visible), congruent with the existence of four σ-holes opposite the Zn−O bonds. The location of the σ-holes coincides with the location of the methoxide group ($-OCH_3$) in the actual complex.

NBO-Based σ-Hole/π-Hole SpB: A True Comparison. In the complex, we are trying to establish the differentiation between the σ- and π-holes' nature more authentically using NBO analysis. It should be observed that a σ-hole[74] is defined as an electron-deficient region situated along the extension of the donor bond. In contrast, a π-hole[75] is also an electron-deficient area present above a planar molecule or planar groups or atoms from a molecule. NBO analysis has been performed at the wB97XD/def2-TZVP level to understand the electronic distribution and rearrangement due to the Zn···O SpB formation. This analysis can effectively differentiate the characteristics between a σ-hole bonded complex and a π-hole bonded complex. Apart from locating the positive electrostatic potential region using MEP, the interaction

https://doi.org/10.1021/acsomega.3c08422
ACS Omega 2024, 9, 1786−1797

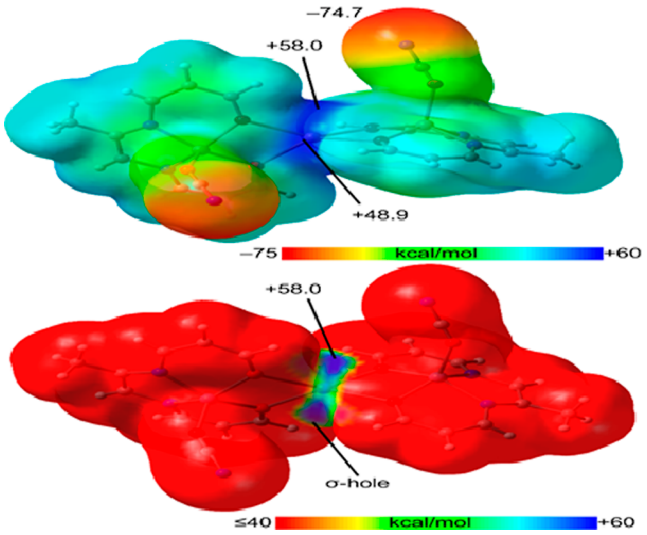

Figure 6. Top: MEP surface of the model of the compound was used to investigate the existence of σ-holes. MEP surface using a different MEP energetic scale. All iso-surfaces have been computed at the PBE0-D3/def2-TZVP (iso-surface 0.001 au). The energies at selected points of the iso-surfaces are given in kcal/mol.

(second-order hyperconjugation energy) of the donor and acceptor orbitals is also a reliable parameter to confirm the class of the nonbonded interaction. Generally, for R−X···A type interaction (where A is the electron donor atom, R can be an atom or any group, and X is an atom associated with a region of positive electrostatic potential), if it is forming through a σ-hole, then a signature LP(A) → σ^*(R−X) orbital interaction is predicted,[76] whereas for interaction through π-hole, an LP(A) → LP*(X) orbital interaction is observed.[77] Previously, Karmakar et al.[27] reported a σ-hole-driven Zn···O intramolecular SpB in two dinuclear Zn(II) complexes. Their claim was solely based on the positive electrostatic potential region along the extension of the Zn−O coordinated bond, and not much was discussed about the orbital interactions. For the present Zn-complex, a second-order hyperconjugation energy of 100.5 kJ/mol is predicted for the LP(O1) → Zn(1) and LP(O2) → Zn(1) interactions. In contrast, an orbital interaction energy of 97.6 kJ/mol is associated with LP(O3) → Zn(1) and LP(O4) → Zn(1) interactions. It should be noted that no LP(O) → Zn−O orbital interaction is predicted for the four nonbonded O···Zn interactions, confirming that these nonbonded contacts are π-hole-based interactions. Therefore, these investigations provide a conclusive idea about the Zn···O π-hole interaction and a criterion that can be utilized to differentiate between a σ-hole or π-hole driven interaction.

CONCLUSIONS

In summary, this article delineates the synthesis, spectroscopic and elemental findings, SEM−EDX characterization, and single-crystal structure analysis of one new trinuclear Zn(II) complex **1**, [{(OCN)Zn(L)}$_2$Zn]. The X-ray structure shows that one terminal Zn(II) center has a square pyramidal geometry, and the central Zn(II) has a tetrahedral geometry. The solid-state crystal structure revealed noncovalent interactions between N···H (15.4%) and O···H (9.1%) contacts, as shown by the Hirshfeld surface and 2-D fingerprint plot. Moreover, the Hirshfeld surface investigates the existence of SpBs between Zn and O-atoms, (Zn···O) contributing to 5.1% of the total interactions. DFT calculations, QTAIM, and NCI plots thoroughly examined the Zn···O SpBs. A σ-hole in central Zn(II) atoms has been evidenced using MEP surfaces. The analysis reveals that these contacts are noncovalent and can be classified as intramolecular SpBs, which can be differentiated between conventional coordination and SpBs by analyzing the QTAIM. Furthermore, the SpBs energy in the complex was estimated using a theoretical model based on complex isomers. Notably, the rare short Zn···O interactions observed in the Zn complex were likely primarily affected by the ligand's organization.

ASSOCIATED CONTENT

Supporting Information

The Supporting Information is available free of charge at https://pubs.acs.org/doi/10.1021/acsomega.3c08422.

Crystallographic information of the complex (CIF)

Representation of sigma hole and core electrons; comparison of the SpB interaction involving tetrahedral and square pyramidal of Zn(II) atom; overview of salen type ligands compartment occupancy by different metal ions; versatile O-bridging fashion of OCN- ions with M^{2+} metal ions; isomers used to estimate the spodium bond energy in the compound; classification of D-A interactions; crystal data and refinement details of complex; some important bond distances (Å) and angles (°) in the complex; EDX analysis of weight (%) contribution of elements and Zn metals; searching previously published spodium bonds; FT-IR spectra for ligand and the complex and for KOCN; Raman spectra for the complex and KOCN; UV-visible spectra for the complex; clubbed ^{1}H NMR spectra of the salen-type ligand and the complex; ^{13}C NMR spectra of the salen-type ligand; EDX profile for the complex; SEM micrographs for the complex; spodium bonds in the complex; QTAIM analysis of the complex; and RI-BP86/def2-TZVP optimized geometry of compound (PDF)

AUTHOR INFORMATION

Corresponding Author

Dhrubajyoti Majumdar − *Department of Chemistry, Tamralipta Mahavidyalaya, Tamluk, West Bengal 721636, India;* orcid.org/0000-0002-9785-7750; Email: dmajumdar30@gmail.com

Authors

Antonio Frontera − *Department de Quimica, Universitat de les Illes Balears, Palma de Mallorca (Baleares) 07122, Spain;* orcid.org/0000-0001-7840-2139

Sourav Roy − *Solid State and Structural Chemistry Unit, Indian Institute of Science, Bangalore 560012, India*

Dipankar Sutradhar − *School of Advanced Sciences and Languages, VIT Bhopal University, Sehore, Madhya Pradesh 466114, India*

Complete contact information is available at: https://pubs.acs.org/10.1021/acsomega.3c08422

Author Contributions

Dr. Dhrubajyoti Majumdar was the project's primary author and conceived the whole research idea, contributed reagents, materials, analysis tools or data, performed data curation,

https://doi.org/10.1021/acsomega.3c08422
ACS Omega 2024, 9, 1786−1797

conceptualization, methodology, research investigation, software visualization, writing review, overall wrote the paper, and completed editing. Dr. Antonio Frontera performed DFT-based experiments and wrote. Dr. Sourav Roy was involved in the single-crystal structure analysis, DFT work, and various crystal structure, graphics preparation, and wrote. Dr. Dipankar Sutradhar performed DFT-based experiments and wrote.

Notes

The authors declare no competing financial interest.

■ ACKNOWLEDGMENTS

This research work has not received funding from any public, commercial, or nonprofit agency. The authors thank Tamralipta Mahavidyalaya's central instrumental laboratory in Tamluk, West Bengal, India, funded by the DST-FIST project (Level-0) under the Department of Science and Technology (DST), Govt. of India. All authors read and approved the final version of the manuscript before submission.

■ REFERENCES

(1) Bauzá, A.; Alkorta, I.; Elguero, J.; Mooibroek, T. J.; Frontera, A. Spodium Bonds: Noncovalent Interactions Involving Group 12 Elements. *Angew. Chem., Int. Ed.* **2020**, *59*, 17482−17487.

(2) (a) Gilli, G.; Gilli, P. *The Nature of the Hydrogen Bond: Outline of a Comprehensive Hydrogen Bond Theory*; OUP: Oxford, 2009. (b) Hobza, P.; Havlas, Z. Blue-Shifting Hydrogen Bonds. *Chem. Rev.* **2000**, *100*, 4253−4264. (c) Scheiner, S. *Hydrogen Bonding: A Theoretical Perspective*; Oxford University Press, 1997. (d) Joseph, J.; Jemmis, E. D. Red-Blue-or No-Shift in Hydrogen Bonds: A Unified Explanation. *J. Am. Chem. Soc.* **2007**, *129*, 4620−4632.

(3) van der Waals, J. D. On the continuity of the gaseous and liquid state. Doctoral Dissertation, University of Leiden, The Netherlands, 1873.

(4) Watson, J. D.; Crick, F. H. C. Molecular structure of nucleic acids: a structure for deoxyribose nucleic acid. *Nature* **1953**, *171*, 737−738.

(5) Riley, K. E.; Hobza, P. On the importance and origin of aromatic interactions in chemistry and bio disciplines. *Acc. Chem. Res.* **2013**, *46*, 927−936.

(6) Lehn, J. M. *Supramolecular Chemistry-Concepts and Perspectives*; VCH: Weinheim, Germany, 1995.

(7) Fujita, M. *Molecular Self-Assembly, Organic versus Inorganic Approaches, Structure and Bonding (Berlin)*; Springer-Verlag: Berlin, Germany, 2000; Vol. *96*.

(8) Steed, J. W.; Atwood, J. L. *Supramolecular Chemistry*; John Wiley & Sons: Chichester, 2000.

(9) Schneider, H. J.; Yatsimirsky, A. *Principles and Methods in Supramolecular Chemistry*; John Wiley & Sons: Chichester, 2000.

(10) Müller-Dethlefs, K.; Hobza, P. Noncovalent interactions: a challenge for experiment and theory. *Chem. Rev.* **2000**, *100*, 143−168.

(11) Janiak, C. A critical account on π-π stacking in metal complexes with aromatic nitrogen-containing ligands. *J. Chem. Soc., Dalton Trans.* **2000**, 3885−3896.

(12) Ran, J.; Wong, M. W. Saturated hydrocarbon-benzene complexes: theoretical study of cooperative CH/π interactions. *J. Phys. Chem. A* **2006**, *110*, 9702−9709.

(13) Riley, K. E.; Pitoňák, M.; Jurečka, P.; Hobza, P. Stabilization, and structure calculations for noncovalent interactions in extended molecular systems based on wave function and density functional theories. *Chem. Rev.* **2010**, *110*, 5023−5063.

(14) Salonen, L. M.; Ellermann, M.; Diederich, F. Aromatic rings in chemical and biological recognition: energetics and structures. *Angew. Chem., Int. Ed.* **2011**, *50*, 4808−4842.

(15) Thakuria, R.; Nath, N. K.; Saha, B. K. The nature, and applications of π-π interactions: a perspective. *Cryst. Growth Des.* **2019**, *19*, 523−528.

(16) Scheiner, S.; Michalczyk, M.; Zierkiewicz, W. Coordination of anions by noncovalently bonded σ-hole ligands. *Coord. Chem. Rev.* **2020**, *405*, 213136.

(17) Alkorta, I.; Elguero, J.; Frontera, A. Not only hydrogen bonds: other noncovalent interactions. *Crystals* **2020**, *10*, 180.

(18) Gomila, R. M.; Frontera, A. Charge assisted halogen and pnictogen bonds: insights from the Cambridge Structural Database and DFT calculations. *CrystEngComm* **2020**, *22*, 7162−7169.

(19) Politzer, P.; Murray, J. S.; Clark, T. σ-Hole bonding: a physical interpretation *Halogen Bonding I: Impact on Materials Chemistry and Life Sciences*; Metrangolo, P., Resnati, G., Eds.; Springer International Publishing, 2015; pp 19−42.

(20) Gomila, R. M.; Bauza, A.; Mooibroek, T. J.; Frontera, A. Spodium bonding in five coordinated Zn(II): a new player in crystal engineering. *CrystEngComm* **2021**, *23*, 3084−3093.

(21) Kumar, P.; Banerjee, S.; Radha, A.; Firdoos, T.; Sahoo, S. C.; Pandey, S. K. Role of non-covalent interactions in the supramolecular architectures of mercury(II) diphenyldithiophosphates: An experimental and theoretical investigation. *New J. Chem.* **2021**, *45*, 2249−2263.

(22) Ghosh, K.; Harms, K.; Bauzá, A.; Frontera, A.; Chattopadhyay, S. σ-Hole halogen bonding interactions in a mixed valence cobalt(iii/ii) complex and anti-electrostatic hydrogen bonding interaction in a cobalt(iii) complex: a theoretical insight. *CrystEngComm* **2018**, *20*, 7281−7292.

(23) Khan, S.; Al Masum, A.; Islam, M. M.; Drew, M. G. B.; Bauzá, A.; Frontera, A.; Chattopadhyay, S. Observation of π-hole interactions in the solid state structures of three new copper(II) complexes with a tetradentate N4 donor Schiff base: Exploration of their cytotoxicity against MDA-MB 468 cells. *Polyhedron* **2017**, *123*, 334−343.

(24) Basak, T.; Roy, S.; Banerjee, S.; Gomila, R. M.; Frontera, A.; Chattopadhyay, S. Synthesis, characterization, and self-assembly of dinuclear zinc Schiff base complexes: A combined experimental and theoretical study. *Polyhedron* **2022**, *225*, 116044.

(25) Mahmoudi, G.; Lawrence, S. E.; Cisterna, J.; Cárdenas, A.; Brito, I.; Frontera, A.; Safin, D. A. A new spodium bond driven coordination polymer constructed from mercury(II) azide and 1,2-bis(pyridin-2-ylmethylene) hydrazine. *New J. Chem.* **2020**, *44*, 21100−21107.

(26) Majumdar, D. J.; Dey, S.; Kumari, A.; Pal, T. K.; Bankura, K.; Mishra, D. Dicyanamide-intertwined assembly of two new Zn complexes based on N_2O_4-type pro-ligand: Synthesis, crystal networks, spectroscopic insights, and selective nitroaromatic turn-off fluorescence sensing. *Spectrochim. Acta, Part A* **2021**, *254*, 119612.

(27) Karmakar, M.; Frontera, A.; Chattopadhyay, S.; Mooibroek, T. J.; Bauzá, A. Intramolecular Spodium Bonds in Zn(II) Complexes: Insights from Theory and Experiment. *Int. J. Mol. Sci.* **2020**, *21*, 7091.

(28) (a) Xia, T.; Li, D.; Cheng, L. Theoretical analysis of the spodium bonds in $HgCl_2\cdots L$ (L = ClR, SR_2, and PR_3) dimers. *Chem. Phys.* **2020**, *539*, 110978. (b) Mahmoudi, G.; Masoudiasl, A.; Babashkina, M. G.; Frontera, A.; Doert, T.; White, J. M.; Zangrando, E.; Zubkov, F. I.; Safin, D. A. On the importance of π-hole spodium bonding in tricoordinated Hg^{II} complexes. *Dalton Trans.* **2020**, *49*, 17547−17551.

(29) Kuppler, R. J.; Timmons, D. J.; Fang, Q.-R.; Li, J.-R.; Makal, T. A.; Young, M. D.; Yuan, D.; Zhao, D.; Zhuang, W.; Zhou, H.-C. Potential applications of metal-organic frameworks. *Coord. Chem. Rev.* **2009**, *253*, 3042−3066.

(30) Janiak, C.; Vieth, J. K. MOFs, MILs and more: concepts, properties, and applications for porous coordination networks (PCNs). *New J. Chem.* **2010**, *34*, 2366−2388.

(31) Adarsh, N. N.; Dastidar, P. Coordination polymers: what has been achieved in going from innocent 4,4′-bipyridine to bis-pyridyl ligands having a non-innocent backbone? *Chem. Soc. Rev.* **2012**, *41*, 3039−3060.

https://doi.org/10.1021/acsomega.3c08422
ACS Omega 2024, 9, 1786−1797

(32) Majumdar, D. J.; Frontera, A.; Gomila, R. M.; Das, S.; Bankura, K. P. Synthesis, spectroscopic findings and crystal engineering of Pb(ii)−Salen coordination polymers, and supramolecular architectures engineered by σ-hole/spodium/tetrel bonds: a combined experimental and theoretical investigation. *RSC Adv.* **2022**, *12*, 6352−6363.
(33) Majumdar, D. J.; Roy, S.; Frontera, A. The importance of tetrel bonding interactions with carbon in two arrestive iso-structural Cd(ii)−Salen coordination complexes: a comprehensive DFT overview in crystal engineering. *RSC Adv.* **2022**, *12*, 35860−35872.
(34) Majumdar, D. J.; Dey, S.; Kumari, A.; Pal, T. K.; Bankura, K.; Mishra, D. Dicyanamide-intertwined assembly of two new Zn complexes based on N_2O_4-type pro-ligand: Synthesis, crystal networks, spectroscopic insights, and selective nitroaromatic turn-off fluorescence sensing. *Spectrochim. Acta, Part A* **2021**, *254*, 119612.
(35) Majumdar, D. J.; Biswas, J. K.; Mondal, M.; Surendra Babu, M. S.; Metre, R. K.; Das, S.; Bankura, K.; Mishra, D. Coordination of N, O-donor appended Schiff base ligand (H_2L^1) towards Zinc(II) in presence of pseudohalides: Syntheses, crystal structures, photoluminescence, antimicrobial activities and Hirshfeld surfaces. *J. Mol. Struct.* **2018**, *1155*, 745−757.
(36) Majumdar, D. J.; Dey, S.; Sreejith, S. S.; Biswas, J. K.; Mondal, M.; Shukla, P.; Das, S.; Pal, T. K.; Das, D.; Bankura, K.; Mishra, D. Syntheses, crystal structures and photo physical aspects of azido-bridged tetranuclear cadmium (II) complexes: DFT/TD-DFT, thermal, antibacterial, and anti-biofilm properties. *J. Mol. Struct.* **2019**, *1179*, 694−708.
(37) Saha, S.; Choudhury, C. R.; Pilet, G.; Frontera, A.; Mitra, S. Design of end-on cyanato bridged trinuclear Cu(II) Schiff base complex with salen type Schiff base ligand: Synthesis, structural investigation and DFT study. *J. Coord. Chem.* **2017**, *70*, 1389−1405.
(38) Mahmoudi, G.; Zangrando, E.; Miroslaw, B.; Gurbanov, A. V.; Babashkina, M. G.; Frontera, A.; Safin, D. A. Spodium bonding and other non-covalent interactions assisted supramolecular aggregation in a new mercury(II) complex of a nicotinohydrazide derivative. *Inorg. Chim. Acta* **2021**, *519*, 120279.
(39) Sheldrick, G. M. *SADABS, a Software for Empirical Absorption Correction, Ver.2.05*; University of Göttingen: Göttingen, Germany, 2002.
(40) *SMART & SAINT Software Reference manuals Version 6.45*; Bruker Analytical X-ray Systems, Inc.: Madison, WI, 2003.
(41) *SHELXTL Reference Manual Ver. 6.1*; Bruker Analytical X-ray Systems, Inc.: Madison, WI, 2000.
(42) Sheldrick, G. M. *SHELXTL, a Software for Empirical Absorption Correction Ver.6.12*; Bruker AXS Inc.: WI. Madison, 2001.
(43) Dolomanov, O. V.; Bourhis, L. J.; Gildea, R. J.; Howard, J. A. K.; Puschmann, H. OLEX2, A complete structure solution, refinement, and analysis program. *J. Appl. Crystallogr.* **2009**, *42*, 339−341.
(44) Ahlrichs, R.; Bär, M.; Häser, M.; Horn, H.; Kölmel, C. Electronic structure calculations on workstation computers: The program system turbomole. *Chem. Phys. Lett.* **1989**, *162*, 165−169.
(45) Weigend, F. Accurate Coulomb-fitting basis sets for H to Rn. *Phys. Chem. Chem. Phys.* **2006**, *8*, 1057−1065.
(46) Bader, R. F. W. A quantum theory of molecular structure and its applications. *Chem. Rev.* **1991**, *91*, 893−928.
(47) Lu, T.; Chen, F. Multiwfn: A multifunctional wavefunction analyzer. *J. Comput. Chem.* **2012**, *33*, 580−592.
(48) Humphrey, W.; Dalke, A.; Schulten, K. VMD: visual molecular dynamics. *J. Mol. Graphics* **1996**, *14*, 33−38.
(49) Chai, J.-D.; Head-Gordon, M. Long-range corrected hybrid density functionals with damped atom-atom dispersion corrections. *Phys. Chem. Chem. Phys.* **2008**, *10*, 6615−6620.
(50) Reed, A. E.; Curtiss, L. A.; Weinhold, F. Intermolecular interactions from a natural bond orbital, donor-acceptor viewpoint. *Chem. Rev.* **1988**, *88*, 899−926.
(51) Frisch, M. J.; Trucks, G. W.; Schlegel, H. B.; Scuseria, G. E.; Robb, M. A.; Cheeseman, J. R.; Scalmani, G.; Barone, V.; Mennucci, B.; Petersson, G. A.; Nakatsuji, H.; Caricato, M.; Li, X.; et al. *Gaussian 09*, Revision C.01; Gaussian, Inc.: Wallingford, CT, 2009.
(52) Spackman, M. A.; Jayatilaka, D. Hirshfeld Surface Analysis. *CrystEngComm* **2009**, *11*, 19−32.
(53) Hirshfeld, F. L. Bonded-atom fragments for describing molecular charge densities. *Theor. Chem. Acta.* **1977**, *44*, 129−138.
(54) Clausen, H. F.; Chevallier, M. S.; Spackman, M. A.; Iversen, B. B. Three new co-crystals of hydroquinone: crystal structures and Hirshfeld surface analysis of intermolecular interactions. *New J. Chem.* **2010**, *34*, 193−199.
(55) Rohl, A. L.; Moret, M.; Kaminsky, W.; Claborn, K.; McKinnon, J. J.; Kahr, B. Hirshfeld Surfaces Identify Inadequacies in Computations of Intermolecular Interactions in Crystals: Pentamorphic 1,8-Dihydroxyanthraquinone. *Cryst. Growth Des.* **2008**, *8*, 4517−4525.
(56) Parkin, A.; Barr, G.; Dong, W.; Gilmore, C. J.; Jayatilaka, D.; McKinnon, J. J.; Spackman, M. A.; Wilson, C. C. Comparing entire crystal structures: structural genetic fingerprinting. *CrystEngComm* **2007**, *9*, 648−652.
(57) Spackman, M. A.; McKinnon, J. J. Fingerprinting intermolecular interactions in molecular crystals. *CrystEngComm* **2002**, *4*, 378−392.
(58) Basak, T.; Gomila, R. M.; Frontera, A.; Chattopadhyay, S. Differentiating intramolecular spodium bonds from coordination bonds in two polynuclear zinc(II) Schiff base complexes. *CrystEngComm* **2021**, *23*, 2703−2710.
(59) Basak, S.; Sen, S.; Banerjee, S.; Mitra, S.; Rosair, G.; Rodriguez, M. G. Three new pseudohalide bridged dinuclear Zn(II) Schiff base complexes: Synthesis, crystal structures and fluorescence studies. *Polyhedron* **2007**, *26*, 5104−5112.
(60) Jena, H. S.; Manivannan, V. Molecular structures of dinuclear zinc(II) complexes of chiral tridentate imine and amine ligands: Effect of ligand geometry on diastereoselectivity. *Inorg. Chim. Acta* **2013**, *394*, 210−219.
(61) Lever, A. B. P., *Inorganic Spectroscopy*, 2nd ed.; Elsevier, New York, 1984.
(62) Nakamoto, K. *Infrared and Raman Spectra of Inorganic and Coordination Compounds: Part B: Applications in Coordination, Organometallic, and Bioinorganic Chemistry*; John Wiley, 2008.
(63) Sadhukhan, D.; Ray, A.; Rosair, G.; Charbonnière, L.; Mitra, S. A Two-Dimensional Zinc(II)−Schiff Base Coordination Polymer Formed by Six-Membered Metallacyclic Repeating Motif: Structural Aspects, Thermal and Photophysical Properties. *Bull. Chem. Soc. Jpn.* **2011**, *84*, 211−217.
(64) Amirnasr, M.; Schenk, K. J.; Salavati, M.; Dehghanpour, S.; Taeb, A.; Tadjarodi, A. Synthesis and Characterization of Cobalt(II), Nickel(II), and Zinc(II) Complexes with N,N ′-bis(Trans-Cinnamaldehyde)-1,2-Diiminoethane Ligand, (ca2en): Crystal and Molecular Structures of Co(ca2en)Cl_2, Co(ca2en)Br_2 and Ni(ca2en)-Br_2. *J. Coord. Chem.* **2003**, *56*, 231−243.
(65) Rabiei, K.; Mohammadkhani, Z.; Keypour, H.; Kouhdareh, J. Palladium Schiff base complex-modified Cu(BDCNH_2) metal-organic frameworks for C-N coupling. *RSC Adv.* **2023**, *13*, 8114−8129.
(66) Roy, S.; Mondal, I.; Harms, K.; Chattopadhyay, S. A trigonal dodecahedral cadmium(II) complex with zinc(II)-salen type metalloligand: Synthesis, structure, self-assembly and application in the detection of various nitroaromatics via turn-off fluorescence response. *Polyhedron* **2019**, *159*, 265−274.
(67) Addison, A. W.; Rao, T. N.; Reedijk, J.; van Rijn, J.; Verschoor, G. C. Synthesis, structure, and spectroscopic properties of copper(II) compounds containing nitrogen−sulphur donor ligands; the crystal and molecular structure of aqua[1,7-bis(N-methylbenzimidazol-2′-yl)-2,6-dithiaheptane]copper(II) perchlorate. *J. Chem. Soc., Dalton Trans.* **1984**, 1349−1356.
(68) Turner, M. J.; Grabowsky, S.; Jayatilaka, D.; Spackman, M. A. Accurate and Efficient Model Energies for Exploring Intermolecular Interactions in Molecular Crystals. *J. Phys. Chem. Lett.* **2014**, *5*, 4249−4255.
(69) Venkatesan, P.; Thamotharan, S.; Ilangovan, A.; Liang, H.; Sundius, T. Crystal structure, Hirshfeld surfaces and DFT computation of NLO active (2E)-2-(ethoxycarbonyl)-3-[(1-me-

https://doi.org/10.1021/acsomega.3c08422
ACS Omega 2024, 9, 1786−1797

thoxy-1-oxo-3-phenylpropan-2-yl) amino] prop-2-enoic acid. *Spectrochim. Acta, Part A* **2016**, *153*, 625−636.
(70) Turner, M. J.; Thomas, S. P.; Shi, M. W.; Jayatilaka, D.; Spackman, M. A. Energy frameworks: insights into interaction anisotropy and the mechanical properties of molecular crystals. *Chem. Commun.* **2015**, *51*, 3735−3738.
(71) Yuan, G.; Shao, K. Z.; Du, D. Y.; Wang, X. L.; Su, Z. M.; Ma, J. F. Secondary ligand-directed assembly of metal-organic coordination polymers based on a 2-(pyridin-4-yl)-1H-imidazole-4,5-dicarboxylic acidligand: Syntheses, structures and photoluminescent properties. *CrystEngComm* **2012**, *14*, 1865−1873.
(72) Orpen, A. G.; Brammer, L.; Allen, F. H.; Kennard, O.; Watson, D. G.; Taylor, R. Supplement. Tables of bond lengths determined by X-ray and neutron diffraction. Part 2. Organometallic compounds and co-ordination complexes of the d- and f-block metals. *J. Chem. Soc., Dalton Trans.* **1989**, S1−S83.
(73) Kumar, P.; Frontera, A.; Pandey, S. Coordination versus spodium bonds in dinuclear Zn(ii) and Cd(ii) complexes with a dithiophosphate ligand. *New J. Chem.* **2021**, *45*, 19402−19415.
(74) Clark, T.; Hennemann, M.; Murray, J. S.; Politzer, P. Halogen bonding: the σ-hole. *J. Mol. Model.* **2007**, *13*, 291−296.
(75) (a) Esrafili, M. D.; Nurazar, R. Chalcogen bonds formed through π-holes: SO_3 complexes with nitrogen and phosphorus bases. *Mol. Phys.* **2016**, *114*, 276−282. (b) Calabrese, C.; Gou, Q.; Maris, A.; Caminati, W.; Melandri, S. Probing the Lone Pair···π-Hole Interaction in Perfluorinated Heteroaromatic Rings: The Rotational Spectrum of Pentafluoropyridine·Water. *J. Phys. Chem. Lett.* **2016**, *7*, 1513−1517.
(76) (a) Sutradhar, D.; Chandra, A. K.; Zeegers-Huyskens, T. A theoretical investigation of the interaction between fluorinated dimethyl ethers and molecular chlorine. *Mol. Phys.* **2014**, *112*, 2791−2801. (b) Sutradhar, D.; Bhattarai, S.; Parveen, S.; Chandra, A. K. Comparison between Chlorine-Shared and π-Halogen Bonds Involving Substituted Phosphabenzene and ClF Molecules. *ACS Omega* **2020**, *5*, 24095−24105.
(77) (a) Bhattarai, S.; Sutradhar, D.; Chandra, A. K. Strongly Bound π-Hole Tetrel Bonded Complexes between H_2SiO and Substituted Pyridines. Influence of Substituents. *ChemPhysChem* **2022**, *23*, No. e202200146. (b) Bhattarai, S.; Sutradhar, D.; Huyskens, T. Z.; Chandra, A. K. Nature and Strength of the π-Hole Chalcogen Bonded Complexes between Substituted Pyridines and SO_3 Molecule. *ChemistrySelect* **2021**, *6*, 7514−7524.

https://doi.org/10.1021/acsomega.3c08422
ACS Omega 2024, 9, 1786−1797